

The relationship between dry rock bulk modulus and porosity – An empirical study

Brian H. Russell¹ and Tad Smith²

ABSTRACT

There are various approaches to computing dry rock bulk modulus as a function of porosity and, from this, inferring velocity and density changes due to reservoir fluid change as a function of porosity. One such approach is the pore space stiffness method. A second approach is the critical porosity model (Mavko and Mukerji, 1995). Using the clean sandstones at different pressures from a dataset collected by Han (1986), and Han et al. (1986), we will evaluate the accuracy of each method. Based on the observations as a function of reservoir pressure, we will also predict an empirical relationship between pore space stiffness and pressure.

INTRODUCTION

Fluid replacement modeling is a procedure whereby the in-situ properties of a reservoir are replaced with alternate values from which seismic parameters such as P -wave velocity, S -wave velocity and density can be computed. The basic equations for P and S -wave velocity in the saturated, porous reservoir can be written as

$$V_{P_sat} = \sqrt{\frac{K_{sat} + \frac{4}{3}\mu_{sat}}{\rho_{sat}}}, \quad (1)$$

$$V_{S_sat} = \sqrt{\frac{\mu_{sat}}{\rho_{sat}}}, \quad (2)$$

where the subscript sat indicates the fluid-saturated case, V_P is the P -wave velocity, V_S is the S -wave velocity, ρ is the density, μ is the shear modulus, and K is the bulk modulus, or the inverse of compressibility. We will assume that the values given in equations (1) and (2) are the observed in-situ values. Our goal is to then compute new values representing alternate reservoir conditions.

In equations (1) and (2), the saturated density can either be measured in-situ or computed from the equation

$$\rho_{sat} = \rho_m(1-\phi) + \rho_w S_w \phi + \rho_g S_g \phi + \rho_o S_o \phi, \quad (3)$$

where the subscripts m , w , g and o indicate matrix, water, gas and oil, S is the fraction of saturation of each fluid component and ϕ is porosity. (Note that even if we measure the in-situ density values, equation (3) will be used in the fluid replacement modeling case).

¹ Hampson-Russell, A CGGVeritas Company, Calgary, Alberta, brian.russell@cggveritas.com

² Hampson-Russell, A CGGVeritas Company, Houston, Texas, tad.smith@cggveritas.com

Once we have the measured or computed saturated density value, the value of the shear modulus in equations (1) and (2) can be computed from the S -wave velocity using equation (2) to give:

$$\mu_{sat} = \rho_{sat} V_{S_sat}^2 \quad (4)$$

The value of the saturated bulk modulus can then be found from equation (1), giving:

$$K_{sat} = \rho_{sat} V_{P_sat}^2 - (4/3)\mu_{sat} \quad (5)$$

Now we proceed to perform fluid replacement modeling. The generally accepted method of doing this is with the Biot-Gassmann equations (Biot, 1941), (Gassmann, 1951), (Mavko et al., 1988). These equations assume that the shear modulus is independent of fluid content (but not porosity, which will be discussed later), or

$$\mu_{sat} = \mu_{dry}$$

where μ_{dry} is the shear modulus of the dry rock, which is the rock for which the pore fluids have been fully evacuated. For the bulk modulus, the Biot-Gassmann equations can be written:

$$\frac{K_{sat}}{K_m - K_{sat}} = \frac{K_{dry}}{K_m - K_{dry}} + \frac{K_{fl}}{\phi(K_m - K_{fl})}, \quad (7)$$

where K_{dry} is the dry rock bulk modulus, K_m is the mineral bulk modulus and K_{fl} is the fluid bulk modulus, normally computed by the Reuss average given by

$$\frac{1}{K_{fl}} = \frac{S_w}{K_w} + \frac{S_g}{K_g} + \frac{S_o}{K_o} \quad (8)$$

(Note that this is for uniform distribution of the fluids. For patchy saturation, we use the linear Voigt average).

There are many alternate forms of the Biot-Gassmann equations besides equation (7), but we have found this form to be the easiest to work with when performing fluid replacement modeling. If we assume that we know the saturated, mineral and fluid bulk moduli, as well as the porosity, then the only unknown in equation (7) is the dry rock bulk modulus. This can then be computed by re-arranging equation (7) to give

$$K_{dry} = K_m \frac{x}{1+x}, \quad (9)$$

Once we have computed K_{dry} , we can change the fluid value by using new saturations in equation (8) and then re-compute K_{sat} and thus ρ_{sat} and V_{P_sat} . For the case of a fluid change only, the shear modulus and dry rock bulk modulus will not change. However, if we want to change the porosity in equation (7), both the dry rock and shear moduli will change. To change these parameters, there is no clear consensus as to which method to use. The first author of this report (BR) has always used a method based on pore stiffness, but this was simply because this was what was suggested by another author

when he first implemented fluid replacement modeling. Mavko and Mukerji (1995) suggest that a better approach is the critical porosity method, and figures in their paper would appear to support this assertion.

The objective of this study is therefore to use the dataset obtained by Han (Han et al., 1986) to determine which of these two methods gives a better fit. First, we will review the theory behind the pore stiffness and critical porosity methods.

PORE STIFFNESS AND CRITICAL POROSITY

To model dry rock bulk modulus at different porosities, one approach is to use pore space stiffness, which is the inverse of the dry rock space compressibility at a constant pore pressure. It can be shown using the Betti-Rayleigh reciprocity theorem (Mavko and Mukerji, 1995) that the pore space stiffness, K_ϕ , is related to the dry rock bulk modulus, the mineral bulk modulus and porosity by the relationship

$$\frac{1}{K_{dry}} = \frac{1}{K_m} + \frac{\phi}{K_\phi} . \quad (10)$$

Note that equation (10) can be re-arranged to give the following relationship

$$\frac{K_{dry}}{K_m} = \frac{1}{1 + \frac{\phi}{k}} , \quad (11)$$

$$k = \frac{K_\phi}{K_m} .$$

where

Equation (11) tells us that the dry rock over matrix bulk modulus ratio is an inverse function of porosity and the pore space stiffness over matrix bulk modulus ratio k . Note first that this equation confirms our observations that we expect this ratio to go to one at zero porosity. Also, it is clear that either as k gets smaller or ϕ gets larger, this ratio gets smaller. This is confirmed in Figure 1, which shows a family of dry rock over matrix bulk modulus ratio curves for varying values of k . The basic idea behind the pore stiffness method is that, for a given pressure, K_ϕ should stay constant over a range of porosities, allowing us to re-compute K_{dry} at a different porosity, ϕ_{new} , using the a re-arrangement of equation (10) given by:

$$K_{dry_new} = \left[\frac{1}{K_m} + \frac{\phi_{new}}{K_\phi} \right]^{-1} . \quad (12)$$

By estimating K_ϕ from the in-situ case, we can therefore compute a new value of K_{dry} at a new porosity.

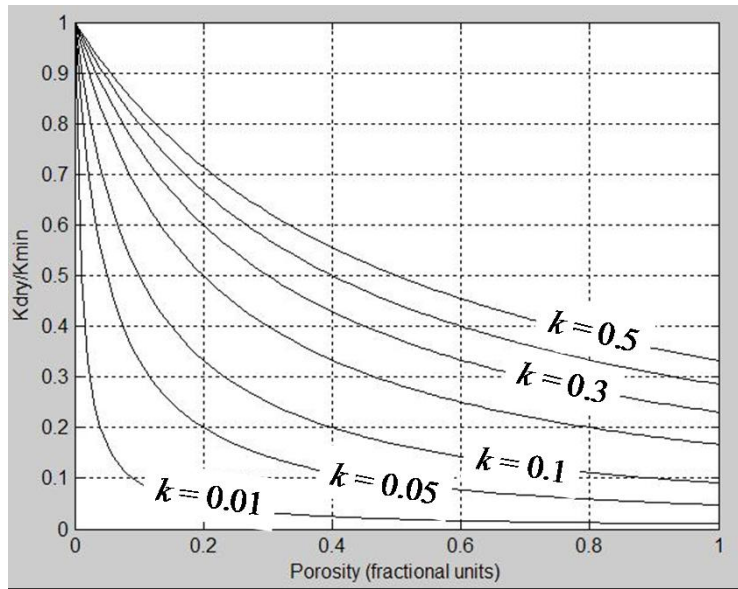


FIG. 1. A family of dry rock over matrix bulk modulus ratio curves for varying values of k .

An alternate approach to changing K_{dry} as a function of porosity is the critical porosity method (Nur, 1992, Mavko and Mukerji, 1995). To understand this approach, let us first consider the upper (Voigt) and lower (Reuss) bounds. As also discussed by Mavko and Mukerji (1995), these two bounds are given by:

$$K_{dry}^{Voigt} = K_m(1-\phi) + K_{air}\phi \approx K_m(1-\phi), \quad (13)$$

and

$$K_{dry}^{Reuss} = \left[\frac{1-\phi}{K_m} + \frac{\phi}{K_{air}} \right]^{-1} \approx 0. \quad (14)$$

Note that the normalized Voigt bound is therefore given as:

$$\frac{K_{dry}^{Voigt}}{K_m} = 1 - \phi. \quad (15)$$

As shown by Nur (1992), high pressure sandstone and glass bead data often show fairly linear trends that can be shown to follow the equation:

$$\frac{K_{dry}}{K_m} = 1 - \frac{\phi}{\phi_c}. \quad (16)$$

where ϕ_c is equal to critical porosity, which is the porosity that separates load-bearing sediments below ϕ_c from suspensions above ϕ_c . Note that this is a scaled version of equation (15).

Figure 2 shows a comparison of the Voigt and Reuss bounds and the critical porosity and constant pore stiffness approaches. Note that the value labeled ϕ_{max} is the point at which the constant pore stiffness curve crosses the Voigt bound. Values above this point would be unrealistic. In fact, the constant pore stiffness curve is really valid only up to porosities much less than this value.

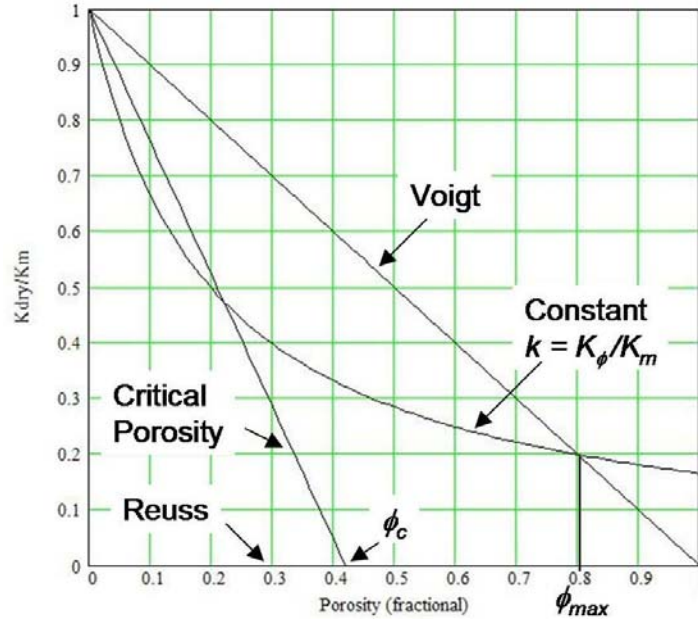


FIG. 2. A comparison of the Reuss and Voigt bounds and the critical porosity and constant K_ϕ curves.

EMPIRICAL STUDY USING HAN'S DATASET

In the previous section, we discussed two valid approaches to modeling K_{dry} as a function of porosity: the pore stiffness method and the critical porosity method. In this section we will evaluate how well they fit a dataset that was measured by De-hua Han for his Ph.D. thesis at Stanford University (Han, 1986). This dataset consisted of 70 separate sandstone samples of varying porosity and clay content (from clean to 51% clay). For each sample, measurements of P -wave velocity, S -wave velocity and density were done for both the wet and dry cases. In addition, the velocities were measured at pressures of 5, 10, 20, 30, 40 and 50 Mpa, respectively. This dataset was used initially by Han to predict the effects of porosity and clay content on the acoustic properties of sandstones (Han et al., 1986). Mavko and Mukerji (1995) use only the ten clean sandstones from Han's dataset in their examples. They use all the sandstones at 40 Mpa, which illustrate a reasonable visual fit to a critical porosity trend, and a single sandstone at pressures from 5 to 40 Mpa, which illustrate the fact that K_{dry}/K_m is pressure dependent. These two sets of points are shown in Figures 3(a) and (b), without any trends superimposed.

In this study, we will perform an analytic study to determine which model gives the best fit to these points: critical porosity or constant pore space stiffness.

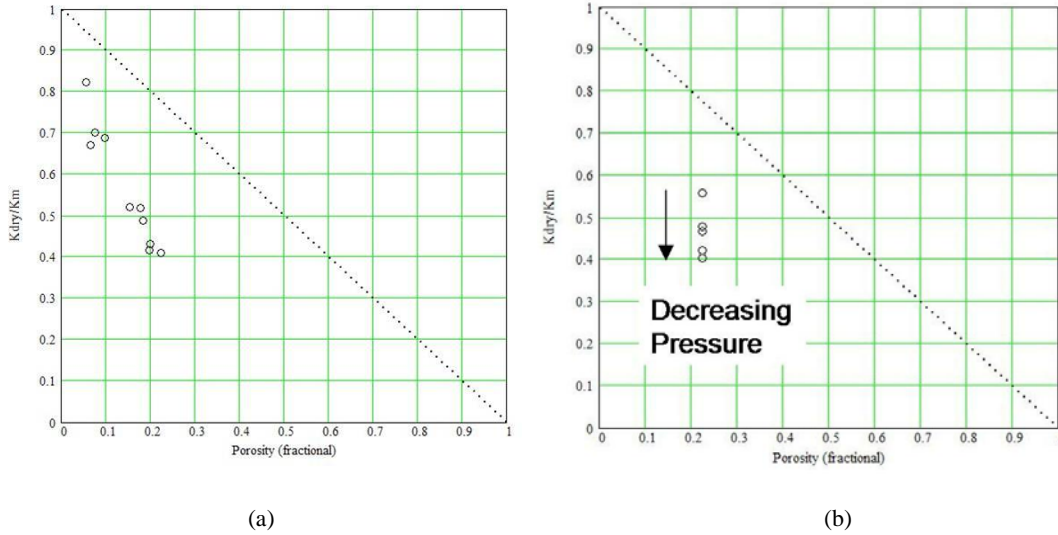


FIG. 3. The clean sandstones from Han’s dataset plotted on the K_{dry}/K_m versus porosity template, where (a) shows all ten sandstones at a pressure of 40 Mpa, and (b) shows a single sandstone at pressures of 5, 10, 20, 30 and 40 Mpa.

First, let us consider the points in Figure 3(a), which represent ten clean sandstones at a pressure of 40 MPa. To fit the constant pore stiffness and critical porosity models to these points, note that both equations (11) and (16) can be fit by the simple linear function given as

$$y = mx \tag{17}$$

where, for the critical porosity model, $y = \frac{K_{dry}}{K_m} - 1$, $m = -\frac{1}{\phi_c}$ and $x = \phi$, and, for the pore space stiffness model, $y = \frac{K_m}{K_{dry}} - 1$, $m = \frac{K_m}{K_\phi}$ and $x = \phi$. The least-squares solution for N points in vector form is given as

$$m = (x^T x)^{-1} x^T y \tag{18}$$

where $x = \begin{bmatrix} x_1 \\ \vdots \\ x_N \end{bmatrix}$ and $y = \begin{bmatrix} y_1 \\ \vdots \\ y_N \end{bmatrix}$, or, in summation form, is given as

$$m = \sum_{i=1}^N x_i y_i / \sum_{i=1}^N x_i^2 \tag{19}$$

For the pore space stiffness method the best fit value was $K_\phi/K_m = 0.162$, and for the critical porosity method the best fit was $\phi_c = 0.343$ (or 34.3%). If we apply these best fit values to the points to get the approximate solution \hat{y} , we can then find the root-mean-square error (*RMSE*) from

$$RMSE = \sqrt{\frac{1}{N} \sum_{i=1}^N (y_i - \hat{y}_i)^2} \quad (20)$$

For the two fits, we found that the *RMSE* for the pore space stiffness method was 0.039, and for the critical porosity method was 0.058. Thus, the critical porosity method is a better fit to these points. The fits are shown in Figures 4(a) and (b).

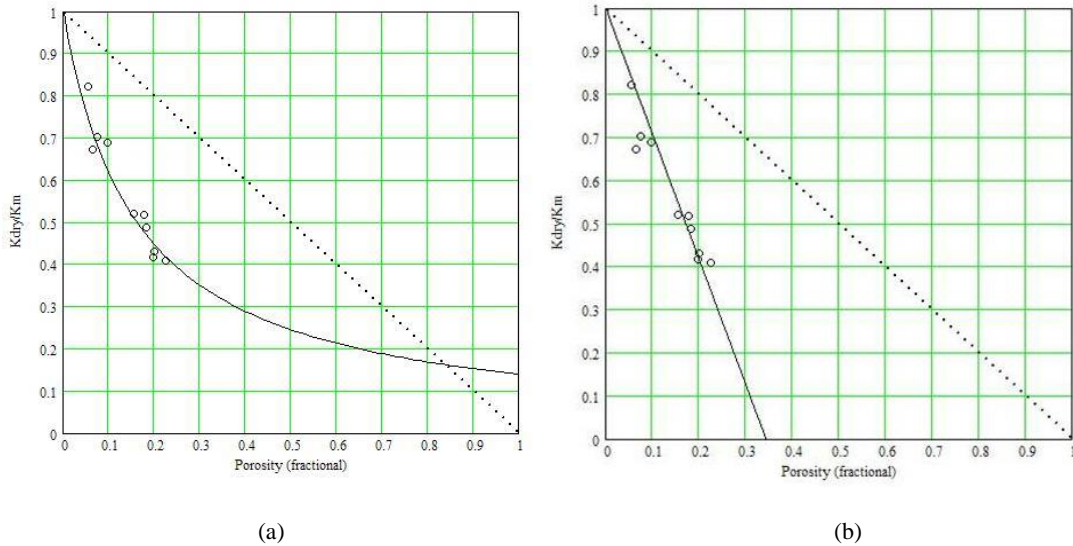


FIG. 4. The best fits for the (a) constant pore space stiffness method, where $K_\phi / K_m = 0.162$, and the RMS error is 0.039, and the (b) critical porosity method, where $\phi_c = 0.343$ (or 34.3%), and the RMS error is 0.058.

If we next turn our attention to Figure 3(b), the single sandstone at different pressures, we find that we can fit different pore space stiffness and critical porosity models to the points. Since constant pore space stiffness and critical porosity values hold only for constant pressures, we would expect a family of curves, as shown in Figures 5(a) and (b). As expected the constant K_ϕ decreases for decreasing pressure, as does ϕ_c .

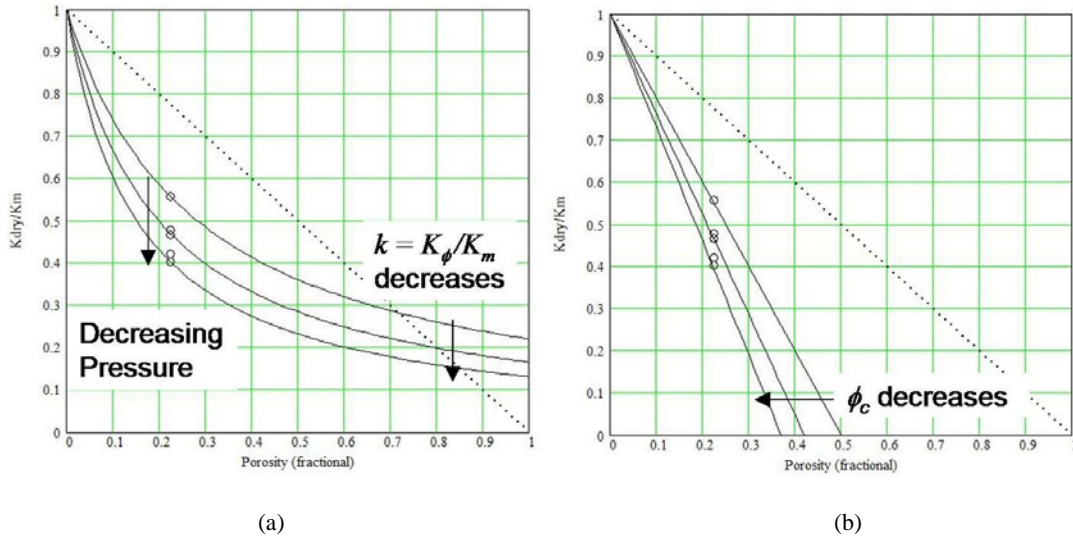


FIG. 5. Curves of decreasing pressure for (a) the pore space stiffness method and (b) the critical porosity method. As expected, both K_ϕ and ϕ_c decrease with decreasing pressure.

However, what we need to do is next is to look at all the values of pressure for each of the clean sandstones and derive a best fit for each set of points.

A PRESSURE VERSUS K_ϕ RELATIONSHIP

We next performed a least squares fit to the full set of ten clean sandstones at each pressure: 5, 10, 20, 30, 40 and 50 Mpa. This is shown in Figures 6(a) and (b) for the lowest (5 MPa) and highest (50 Mpa) pressures.

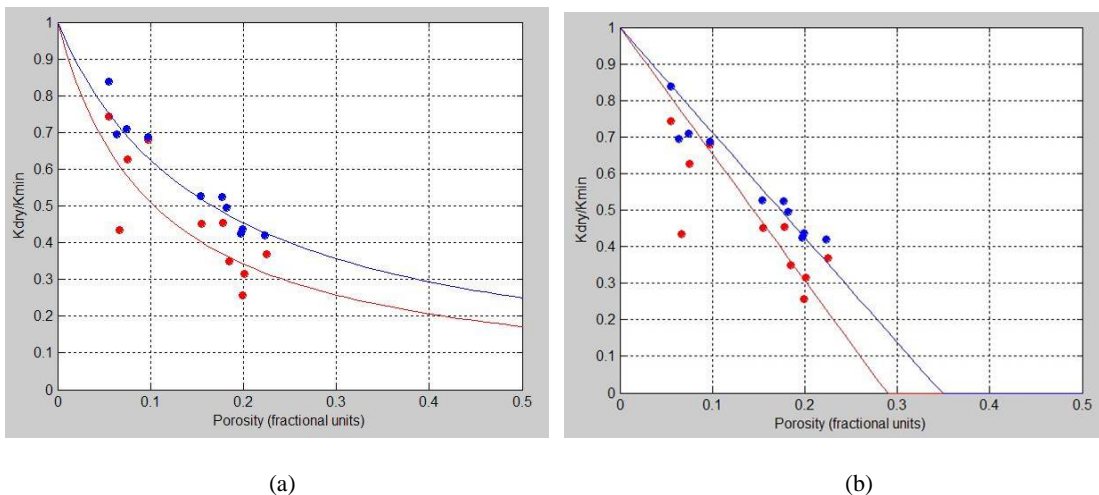


FIG. 6. The best fit curves for pressures of 50 MPa (top curve in blue) and 5 MPa (bottom curve in red) for (a) the pore space stiffness method and, (b) the critical porosity method.

The best fit values and RMS errors for each of the six pressure relationships is shown in Table 1. As can be seen in the table, the error is smaller for the pore space stiffness method in each case, and the values of pore space stiffness and critical porosity increase with increasing pressure, as we expect.

Table 1. The best fit values and RMS errors as a function of pressure for the critical porosity and pore space stiffness methods

$P(\text{MPa})$	ϕ_c	$RMSE$	K_ϕ/K_m	$RMSE$
5	0.289	0.126	0.104	0.094
10	0.311	0.107	0.129	0.076
20	0.329	0.079	0.147	0.055
30	0.338	0.069	0.156	0.044
40	0.343	0.058	0.162	0.039
50	0.348	0.053	0.166	0.038

Obviously, we can produce a fit to either the critical porosity or pore space stiffness values. But, since the pore space fitness curves produce a better least-squares fit to the data, we will focus on deriving a relationship between those values and pressure. Figure 7(a) shows the fit of K_ϕ/K_m versus pressure on a linear scale and Figure 7(b) shows the fit of K_ϕ/K_m versus pressure on a semi-logarithmic scale, where the natural logarithm of pressure has been plotted on the horizontal axis. Note that the logarithmic fit is close to linear, and a best-fit linear fit has been applied. The coefficients for this fit are

$$\frac{K_\phi}{K_m} = 0.065 + 0.027 \ln(P) \tag{21}$$

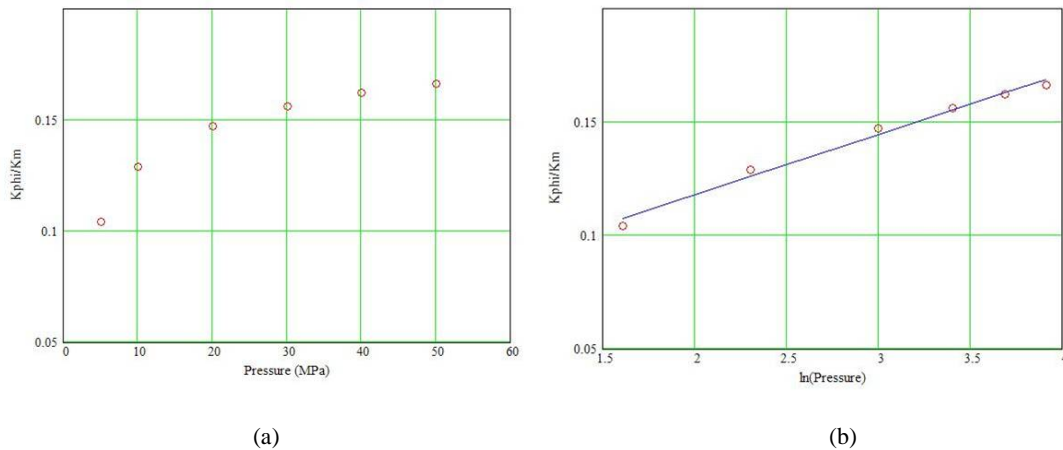


FIG. 7. The constant K_ϕ/K_m fits as a function of pressure plotted on (a) a linear-linear scale and (b) a linear-logarithmic scale. Note the good linear fit in (b).

Note that since equation (21) involves a logarithm, we can use calculus to differentiate this equation and get:

$$\frac{dK_\phi}{dP} = \frac{0.027 K_m}{P} \tag{22}$$

Replacing the derivative with the difference operator and re-arranging, we then find:

$$\Delta K_{\phi} = 0.027 K_m \frac{\Delta P}{P} . \quad (23)$$

Equation (23) is a very useful result, since it allows us derive constant K_{ϕ} curves at different pressures than the in-situ pressure, and hence predict a depth variable K_{dry} versus porosity relationship.

FLUID REPLACEMENT MODELING

Now let us apply the fluid and porosity methods of substitution that we have discussed in the last two sections to a typical sand, for a range of porosities and fluids. For fluid substitution, we will use Biot-Gassmann, as described in the Introduction. For the porosity change, we will use the constant pore space stiffness method. The one item we have not addressed is the way in which shear modulus is changes as a function of porosity. As shown empirically by Murphy et al. (1993), the modulus ratio K_{dry}/μ is remarkably constant for clean sandstones over a range of porosities. The authors found a value of 0.9 for this ratio. Assuming that this ratio is constant, regardless of its value, once we have computed the in-situ and new values of K_{dry} , we can compute a new value for the shear modulus by the equation:

$$\mu_{new} = \mu_{in-situ} \frac{K_{dry_new}}{K_{dry_in-situ}} . \quad (24)$$

Fluid replacement modeling for a wide range of porosities (0 to 50%) and fluids (100% wet to 100% gas) is shown in Figure 8 for a variety of combinations of parameters, including Poisson's ratio versus P -wave velocity, V_p/V_s ratio versus P -wave velocity, V_p/V_s ratio versus P -impedance, and V_p versus V_s .

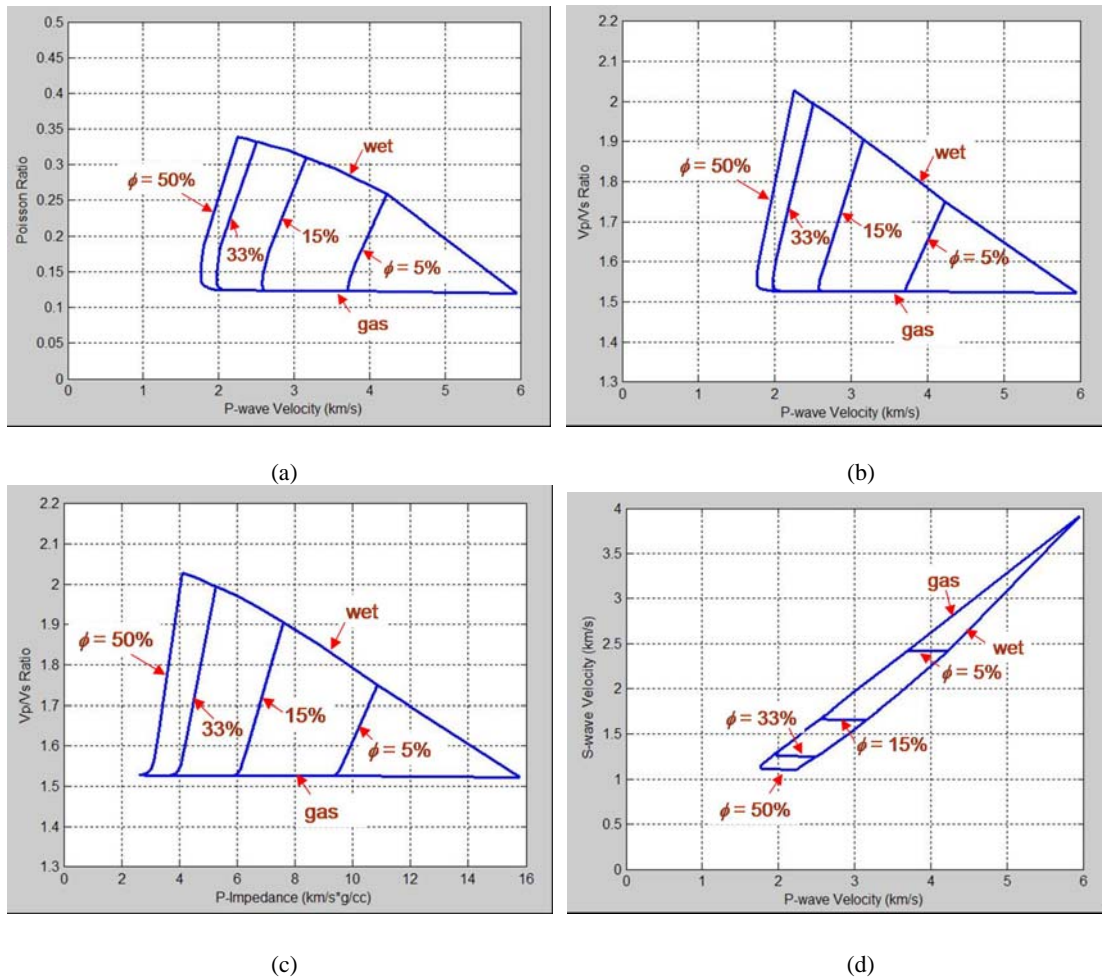


FIG. 8. Fluid replacement modeling for a gas sand with S_w ranging from 100% (wet) to 0% (gas) and for porosities ranging from 0% to 50%, where (a) shows Poisson's ratio versus P -wave velocity, (b) shows V_P/V_S ratio versus P -wave velocity, (c) shows V_P/V_S ratio versus P -impedance, and (d) shows V_P versus V_S .

In Figure 8, note that the key observation is that Poisson's ratio or V_P/V_S ratio is the key indicator of fluid content, whereas P -wave velocity or impedance is the key indicator of porosity. It should be pointed out that the pore space stiffness method that was used in the plots to compute porosity change should probably not be used over as wide a range as shown. But, in this case, note that most of the changes are seen in the low porosity range, so pushing the limits of the model is probably not hurting us too much.

CARBONATE EXAMPLE

Conventional wisdom tells us that the pore space stiffness method works best for unconsolidated sandstones. However, Baechle et al. (2006) found that they could use this method to differentiate between vuggy porosity and microporosity in a carbonate. The authors made 288 ultrasonic measurements from six separate pure carbonate provinces and found that sonic velocity was not only dependent on total porosity, but also on pore type.

Figure 9, which is taken from a paper given by Baechle at “The sound of geology” workshop in Bergen, Norway, shows quite clearly that these two trends of points can be separated using the pore space stiffness method. The authors of this study used the term α for K_ϕ/K_{dry} (which we called k), and find that an α value of 0.1 fits the carbonates that display microporosity and an α value of 0.2 fits the carbonates that display vuggy porosity (the red circles in the figure). The authors conclude that microporosity reduces pore stiffness whereas vuggy porosity creates higher pore stiffness at a given porosity. Note also that the dashed line on the figure is the critical porosity model, which does not clearly separate the two porosity trends.

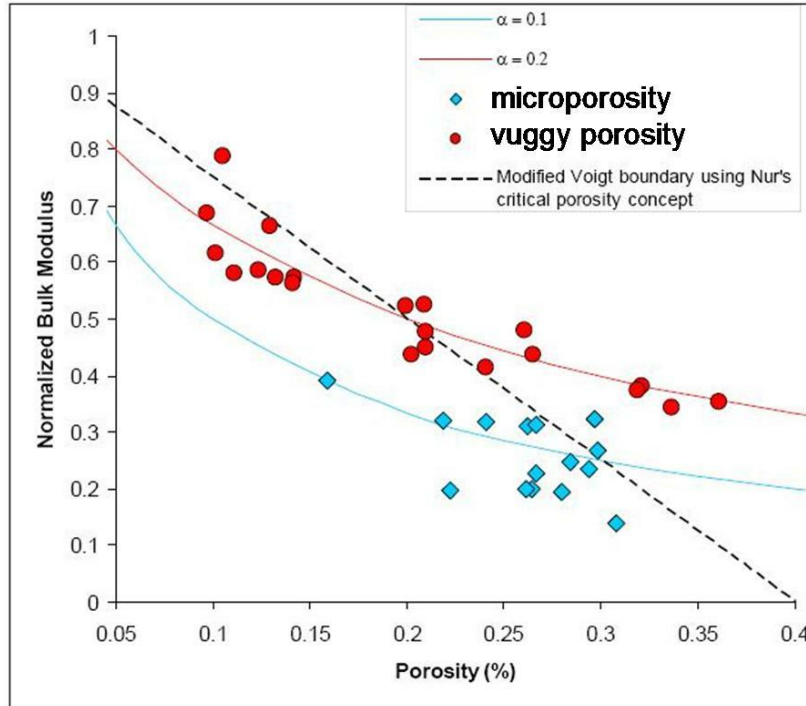


FIG. 9. The use of the pore space stiffness method to discriminate vuggy porosity from microporosity in carbonate ultrasonic measurements.

EMPIRICAL FITS

The two methods that we have discussed, constant pore space stiffness and critical porosity, assume that our data will fit neatly into one or the other model. However, as we have seen, most data will not fit either model perfectly. For that reason, Smith (2007) suggests that empirical fits can be done to either the computed dry rock bulk modulus or the computed shear modulus as a function of porosity. This is shown for a set of sandstones of various porosities and shale content in Figure 10. Both fits were done with the function given by

$$M = a\phi^2 + b\phi + c, \tag{25}$$

where M is the particular modulus.

Note that K_{dry}/μ ratio converges to 1.0 as the shale content goes down, close to the value predicted by Murphy et al. (1993). However, for large shale content, the ratio is equal to values as high as 1.6, suggesting that our assumption that the ratio is constant is not valid in shaly sands.

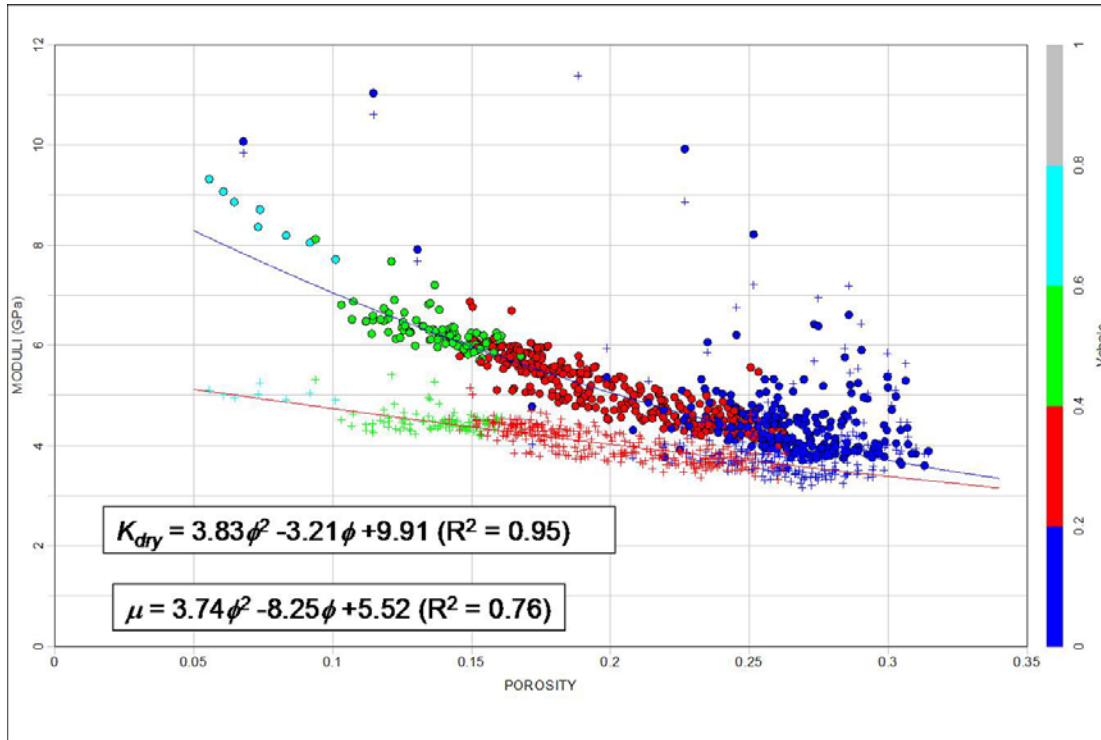


FIG. 10. Empirical fits to K_{dry} and μ for a variety of sandstones of differing porosities and shale content. The correlation coefficient is given as R^2 .

CONCLUSIONS

In this study, we evaluated two different approaches to the modeling of K_{dry} versus porosity in clean sands: the pore space stiffness method and the critical porosity method. Both methods were evaluated using the clean sandstones measured by Han (1986). We found that a useful display and analysis tool was the K_{dry}/K_m versus porosity template proposed by Mavko and Mukerji (1994). For the range of porosities found in the Han sandstones, the pore space stiffness method gave a closer fit than the critical porosity method. By performing fits over a range of different pressures, we were then able to derive a relationship between pressure and constant pore space stiffness, and hence between K_{dry} and porosity at different pressures or depths. Work by Baechle et al. (2007) as also shown that the pore space stiffness method can be used to differentiate microporosity from vugular porosity in carbonates.

However, data compiled by Smith (2007) shows that this approach may start to break down in shaly sands. Also, the method should not be pushed to too high or low porosity limits, and probably works best in the range found in the Han samples, between about 8 and 22%.

ACKNOWLEDGEMENTS

We wish to thank our colleagues at the CREWES Project and at CGGVeritas and Hampson-Russell for their support and ideas, as well as the sponsors of the CREWES Project. We also thank Dr. De-hua Han for providing his complete dataset for our use.

REFERENCES

- Baechle, G.T., Weger, R., Eberli, G.P., and Colpaert, A., 2006, Pore size and pore type effects on velocity – Implications for carbonate rock physics models: Abstract of paper presented at the “Sound of Geology” workshop in Bergen, Norway.
- Biot, M. A., 1941, General theory of three-dimensional consolidation: *Journal of Applied Physics*, **12**, 155-164.
- Gassmann, F., 1951, Uber die Elastizitat poroser Medien: *Vierteljahrsschrift der Naturforschenden Gesellschaft in Zurich*, **96**, 1-23.
- Han, D., 1986, Effects of porosity and clay content on acoustic properties of sandstones and unconsolidated sediments: Ph.D. dissertation, Stanford University.
- Han, D.H., A. Nur, and D. Morgan, 1986, Effects of porosity and clay content on wave velocities in sandstones: *Geophysics*, **51**, 2093-2107.
- Mavko, G., Mukerji, T., and Dvorkin, J., 1998, *The Rock Physics Handbook – Tools for seismic analysis in porous media*: Cambridge University Press.
- Mavko, G., and T. Mukerji, 1995, Seismic pore space compressibility and Gassmann's relation: *Geophysics*, **60**, 1743-1749.
- Murphy, W., Reischer, A., and Hsu, K., 1993, Modulus Decomposition of Compressional and Shear Velocities in Sand Bodies: *Geophysics*, **58**, 227-239.
- Nur, A., 1992, Critical porosity and the seismic velocities in rocks: *EOS, Transactions American Geophysical Union*, **73**, 43-66.
- Smith, T., 2007, *Applied rock properties*: Unpublished course notes from course presented at Doodletrain 2007, Calgary, Alberta.